Eur J Dermatol 2008; 18 (6): 617-31

Jitendrakumar K. PATEL[1]
Sailesh KONDA[2]
Oliver A. PEREZ[2]
Sadegh AMINI[2]
George ELGART[2]
Brian BERMAN[3]

[1] Jamaica Hospital Medical Center, Department of Medicine, Jamaica, NY 11375
[2] University of Miami, Miller School of Medicine, Department of Dermatology and Cutaneous Surgery, 1600 NW 10th Avenue, RMSB, Room 2023A (R250), Miami, FL 33136
[3] University of Miami, Miller School of Medicine, Department of Dermatology and Cutaneous Surgery, 1600 NW 10th Avenue, RMSB, Room 2023A (R250), Miami, FL 33136

Reprints: J.K. Patel <drjitupatel@yahoo.com>

Article accepted on 14/4/2008

Newer technologies/techniques and tools in the diagnosis of melanoma

A number of non-invasive approaches have been developed over the years to provide an objective means of evaluating and diagnosing skin melanoma. However, the current gold-standard in melanoma diagnosis is the examination of a skin lesion by the trained eye of a physician followed by histological examination of an invasive excisional biopsy of the skin specimen. Diagnosis of melanoma by simple visual examination is incorrect in almost 1 out of every 3 melanoma diagnoses. Therefore, the diagnosis of early stage in-depth melanoma by non-invasive methods remains an active area of research. Recent advancements in computer and digital technology have provided several sensitive tools to evaluate the different characteristics of a melanoma lesion including its contour, edge, color, size, depth, and/or elevation. These tools include (1) digital imaging systems and computer analysis instruments such as MoleMax™, SIAscope™, SolarScan®, MelaFind™; (2) tape stripping mRNA; (3) laser-based technology such as Confocal scanning laser microscopy (CSLM), optical coherence tomography (OCT), laser Doppler perfusion imaging (LDPI), (4) Ultrasonography, and (5) other imaging tools such as electrical bio-impedance, MRI and PET scan. The ultimate goal of all investigational instrumentation is the prevention of unnecessary biopsies and a decrease in the prevalence and morbidity associated with malignant melanoma.

Key words: melanoma, dermoscope, ultrasound, MRI, PET scan, digital image analysis

While the development of melanoma may be unpredictable, its prognosis is directly linked to the stage of the disease. Periodic skin examinations have allowed early melanoma detection and improved the prognosis of this disease [1]. However, differentiating early melanoma lesions from other pigmented skin lesions (PSLs) is difficult and diagnosing melanoma by simple visual examination with the ABCD rule is incorrect in almost 1 out of every 3 melanoma diagnoses [2-4]. Dermatologists are now equipped with the dermoscope, the non-invasive handheld microscope for differentiating PSLs from melanocytic lesions *(table 1)*. The dermoscope has a magnifying lens and a light source to illuminate the visual field and a transparent medium of clear oil or gel may be applied on the skin for better visualization. However, the dermoscope is limited in the diagnosis of early melanomas that do not exhibit classic features [5-8]. Binder *et al.* have suggested the epiluminescence microscope (ELM) technique increases sensitivity in formally trained dermatologists, but noted this may decrease diagnostic ability in dermatologists without training [9].

Melanocytic lesions can also be evaluated with the Woods lamp, which emits ultraviolet light at a wavelength of 360, and even by sniffer dogs on the basis of odor [10-15].

Table 1. Dermoscopes and theirs features

Dermoscope	Company	Features	Price
DermLite Platinum® DermLite 100® DermLite Foto® DermLite *PRO*®	3Gen,LLC USA (www.dermlite.com, www.3GenLLC. com)	10-32×, non-contact type, LED* source, handheld	$ 375-1,000
Mini 2000 Dermoscope® Delta 10® Delta 20® Alpha+®	HEINE Optotechnik, Germany (www.heine.com)	10× magnification, handheld, Large High resolution images capacity, contact type. Delta 20(3 or 6-LED, attachable camera) Delta 10 & Alpha+ (XHL Xenon Halogen technology)	$ 300-1,100
DermoGenius® basic II	LINOS Photonics, Inc. MA www.dermogenius.com www.linos.com	10× magnification, handheld, 6 diodes for optimum illumination, two light sources (100% & 70%), adapter for digital camera	$ 700-800

**LEDs: Light Emitting Diodes.*

doi: 10.1684/ejd.2008.0508

However, all these techniques as described above are dependent on the skill of the examiner and can often lead to the biopsy of benign PSLs and potential disregard of malignant ones [16]. Additionally, biopsies are invasive, cannot be performed in every suspected lesion and may have side effects that hinder follow-up studies. In order to decrease the number of excessive invasive biopsies and the potential for subjective human error, we searched for new and non-invasive morphological techniques and tools to assist in the diagnosis of melanoma in its early stages. Such tools include digital imaging systems and computer analysis instruments like MoleMax™, SIAscope™, SolarScan, MelaFind™, tape stripping mRNA, ultrasonography, MRI and PET scan; laser- based technology like Confocal scanning laser microscopy (CSLM), optical coherence tomography (OCT), laser doppler perfusion imaging (LDPI); and electrical bio-impedance. A search of the literature from the period between 1970 and 2007 was performed using PubMed, Medline and Google and relevant articles, as well as pertinent articles from each of their bibliographies which were reviewed without any language restriction. The search criteria were all new non-invasive technologies useful for diagnosing melanoma, availability of sensitivity and specificity of methods, discussion of advantages and disadvantages of each method, and the capability of producing good images. Studies that detected skin cancers other than melanoma or had a paucity of supporting scientific data were excluded.

Digital image capturing and computer processing/analysis

Various dermoscopic instruments utilize a digital camera or a built-in image capturing system for photographing PSLs. Digital image capturing allows for non-deteriorating images with excellent quality and a numerical format that permits objective measurements and teleconsultation [17]. Digital dermoscopy analysis systems can attain resolutions of up to 1,280 × 1,024 pixels, with images acquired *in vivo* at 15 to 25 photograms. Commercially available digital cameras can attain resolutions up to 3,000 × 2,000 pixels but are inadequate because images can be viewed at full resolution only after they have been saved and not in real time [18]. Due to these great advances in optical resolution, dermoscopy remains a quantifiable, easily applicable and reproducible diagnostic tool to help make PSLs with unclear malignant potential a manageable disease [19].

After an image of the PSL is captured, the computer recognizes the pigmented border of the lesion by processing it via segmentation and border extraction [20-23]. The software then measures the degree of asymmetry, border irregularity index, hue, quantity and changes in colors, textures, diameter, perimeter, length, area, internal color distributions, and linear diameter [24-26]. This allows for algorithms to factor the weight of each component in the formulation of a diagnosis and provide an objective analysis of a PSL, which can be compared to previously taken images of the same lesion or the standard software PSL image [27]. The computer software has the ability to provide a diagnosis after evaluating the data, which avoids the potential for subjective human error.

Some systems can also objectively evaluate pigmented cutaneous lesions by artificial neural networks (ANNs) [6, 28, 29]. ANNs are mathematical networks based on a biologic neural system that may be implemented as a computer software program. ANNs have powerful modalities for the recognition of complex patterns, with the ability to maintain accuracy even when confronted with missing or inaccurate data which are not readily apparent to human analysis [30]. The functioning ANNs knowledge is self-learning and uses its experiences from previous input data (*i.e.* melanocytic lesions) to analyze new data. Although ANNs have traditionally been used in engineering, researchers are now applying them to medicine to help doctors analyze, model, and make sense of complex clinical data. ANNs do not require any specific criteria for the diagnosis and function independently of the physician's knowledge, so the inexperienced user can screen PSLs [30, 31]. With the help of these digital imaging and computer analysis techniques, sensitivity and specificity levels can be reached which are near or better than those of expert dermatologists [32-35].

MoleMax™ (Derma Medical Systems, Vienna, Austria) is based on the light polarization technique of dermoscopes [36]. There are two types of MoleMax™ available, with MoleMax I™ containing only one camera and MoleMax II™ having a two camera system, which is particularly helpful for continuous use by different users. The polarized light source is used with the handheld ELM for close-up imaging and does not require any oil immersion or contact fluids between the skin and ELM. ELM images are automatically transferred, allowing for continuous real-time documentation of PSLs with the examination process [36]. The MoleMax I™ software is conducive for follow-up examinations as the *transparent overlay* feature performs a standardized comparison of images with previous data. Apart from live videoscopy, MoleMax™ has a CD-ROM based technology that allows total body photography to create a digital map of the patient's skin for patients with high risk factors and large PSLs. Physician use the stored images in the CD-ROM as a baseline comparison when suspicious changes are found and also for follow-up melanoma screening visits.

Spectrophotometric Intracutaneous Analysis (SIAscope™, Astron Clinica, Cambridge, UK) is a fast, non-invasive and safe method for the diagnosis of PSLs up to 2 mm. This high resolution instrument visualizes the skin structure, vascular composition and reticular pigment networks with detail and clarity, attaining up to 96% sensitivity [37, 38]. There are two methods of SIAscopy, contact and non-contact. Contact SIAscopy utilizes a hand held scanner (SIAscanner) that is placed directly on skin surface of interest before scanning it with light. In non-contact SIAscopy the skin is not touched. A digital camera with a special filter is used to produce images of larger areas of skin. Both methods generate SIAgraphs, computer-generated images that show the distribution of major skin components (melanin, collagen and blood) [37]. The SIAscope™ is based on the principle that individual skin components vary in their optical properties. The device emits harmless radiation ranging from 400 to 1,000 nm into an area of skin with dimensions of 24 × 24 mm or 12 × 12 mm and then measures the reflected light quantity for each wavelength [33, 38]. Skin and its components absorb and/or reflect light to various degrees and can interact preferentially with particular wavelengths of light. The SIAscope™ extracts information regarding the location, quantity and distribution of the

skin and its chromophores, including melanin, collagen, and hemoglobin (*i.e*. vascularity) within the epidermis and papillary dermis, producing eight narrow-band spectrally filtered images, and then displays a characteristic SIAscopic image *(figure 1)*. The data are then displayed via SIAgraphs, which are graphical representations of the digital information [38]. These chromophore wavebands may be removed to view only the melanoma diagnostic information on the graph. These simple features were found to be highly specific (up to 87%) and sensitive (up to 96%) for melanoma [38]. Moncrieff *et al.* studied 348 lesions over a 12 month period with the SIAscope™ and found it to be highly specific (80.1%) and sensitive (82.7%) [33].
SolarScan® is an automated instrument (Polartechnics Ltd, the Sydney Melanoma Unit and CSIRO) for the diagnosis of primary melanoma. It has a three charge-coupled device (CCD) video camera for acquiring digital images of lesions, which can be compared with an empirical database of more than 1800 benign and malignant lesions. Oil is placed on the lesion to eliminate surface reflections and the remote-head camera takes 24-bit, 760 × 570-pixel images with each pixel capturing a 32 × 32 µm area of the skin [39-41]. The fiber optic light source is coupled to a halogen lamp with a color temperature of 3,000 °K. The calibration procedure consists of white balance, black balance, shading correction, dynamic range, and image capture of a reference surface of known reflectivity [39]. In addition to the session-level calibration, the system also has image-level calibration, which is facilitated by 4 gray-scale calibration targets present in each image. The resolution of each of these images is 64 µm per pixel (× 6.2 screen magnification) [39]. Changes in color, pattern and size are recorded along with the position of each monitored lesion on a graphical map of the patient's body. Images of a lesion from different time points can be viewed simultaneously and the corresponding analysis is displayed on four different graphs. The SolarScan® software can automatically select a computerized border for each lesion photo or the user can select one of the three border selection methods to assist the computer with lesion analysis *(figures 2A-B)*. The three-chip camera and color calibration ensures accurate detection of up to 14 shades of dermatoscopic colors, as well as the specific color of Blue-White veil, which is extremely useful for invasive melanoma diagnosis, with a specificity of 97% [39]. Preliminary data suggest that its performance is comparable or superior to that of clinician groups [24, 39, 40]. In the multicenter study of SolarScan, SW Menzies *et al.* studied 2,430 PSLs and found that SolarScan® has 91% sensitivity and 68% specificity, which is comparable or superior to expert diagnosis [24].

MelaFind™ (Electro-Optical Sciences Inc., NY) is a multispectral digital dermoscope with a specialized imaging probe and software to assist with differentiation between early melanoma and other PSLs. Filtered white light from a stable source is transmitted to the skin by a fiber optic illuminator controlled by the computer. After the CCD camera has detected 10 different, narrow-spectrum wavelength bands including visible and infrared light, a multispectral sequence of digital images 1,280 × 1,000 pixels in size is produced in less than 3 seconds [34]. Afterwards, each sequence of multi-spectral images is analyzed for wavelet maxima, asymmetry, color variation, perimeter changes, and textures changes, the software assists with a differential diagnosis [35]. Images are obtained with the MelaFind™ digital dermoscope gray-scale with 1024-level intensity resolution and are produced in each of 10 spectral bands ranging from 430 nm to 950 nm controlled by narrow interference filters on a rotating wheel [42]. Each image has more than 1 million pixels within a 2 × 2 cm visual field, and each pixel is approximately 20 µm [34]. The acquired images are stored without loss of resolution and identified with headers that record wavelength and exposure. Initial studies demonstrated that MelaFind™ can achieve 95% to 100% sensitivity and 70% to 85% specificity [34, 35].

The Fotofinder dermoscope, DermDOC™ is an example of a video dermoscope attached to a digital camera system [36]. It can provide high quality images, variable magnification, macro and micro application, and analytical capability. However, video dermoscopes are at a disadvantage compared to cameras because they lose image resolution after conversion to images.

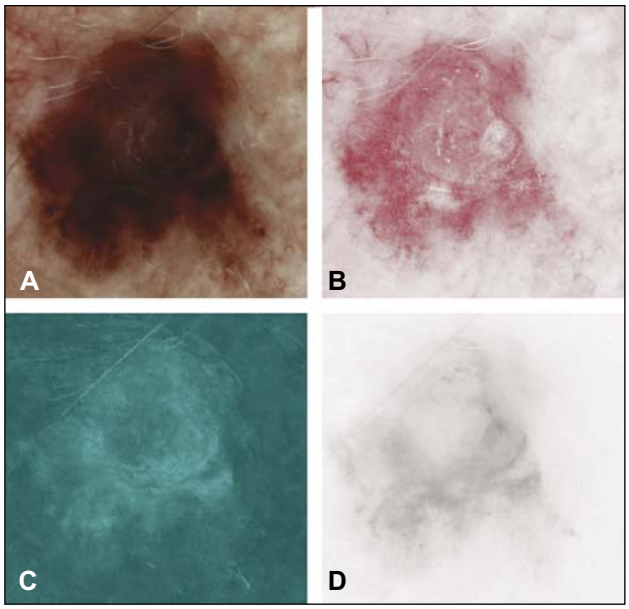

Figure 1. SIAscopic image of an invasive melanoma with different skin chromophores(Used with permission of Astron Clinica, Ltd, Cambridge, United Kingdom). **A)** Invasive Melanoma. **B)** Hemoglobin.**C)** Collagen. **D)** Melanin.

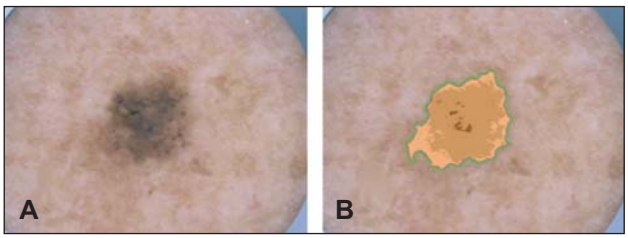

Figure 2. The SolarScan software detects shape and border of a pigmented lesion (Used with permission of Polarthechnics Ltd, Erskineville, Australia). **A)** Pigmented lesion. **B)** Lesion shape and borders detected and analyzed with color segmentation.

Tape stripping mRNA method

Tape stripping is an established and non-invasive method that allows for the recovery of cells comprising the upper epidermis. An adhesive tape is applied to PSLs, briskly rubbed on in a circular motion, and the border of the lesion is demarcated on the tape with a surgical marker. As the tape is removed, superficial cell layers of the stratum corneum (SC) are stripped off and RNA is harvested from these skin samples. The marker demarcation allows for the removal of tape that contacted normal epidermis during processing for mRNA extraction. This yields enough mRNA for analysis by ribonuclease protection assay (RPA) to differentiate melanoma from benign lesions based on gene expression profiles [43]. A study evaluating 150 suspicious pigmented lesions found the tape-stripping toluidine blue method to have a sensitivity of 68.7% and a specificity of 74.5%, demonstrating its potential as a helpful diagnostic tool for the early detection of melanoma [44]. DermTech's (La Jolla, CA) Epidermal Genetic Information Retrieval (EGIR™) technology is the commercialized form of this nucleic acid retrieval process and relies on the use of a custom adhesive film to sample the surface layer of skin. The EGIR™ technique has the advantage of being non-invasive, rapid and easy to perform, painless, and practical for virtually any skin surface. EGIR™ technology also has the advantage of being able to retest the same lesion, leading to a more accurate diagnosis of melanoma and reducing the need for painful biopsies. In a study by Wachsman and colleagues, suspicious pigmented lesions were tape stripped four times using EGIR™ and then biopsied as per standard of care. Normal, uninvolved skin was also tape stripped to serve as the negative control. They found a 20-gene classifier that discriminated melanoma from atypical nevi and subsequent testing of this classifier found it to be 100% sensitive, 90.6% specific and 92.4% accurate for detection of both *in situ* and invasive melanoma [45, 46]. Additional clinical trials are currently underway to finalize candidate gene expression profiles for identifying early stage melanomas.

It is important to note that tape stripping is not expected to substitute for necessary biopsies. Tape stripping is most beneficial as a pre-screen for suspicious pigmented lesions. If an RPA comes back positive for a particular gene expression profile associated with melanoma, the pigmented lesion should be excised and the depth determined.

Ultrasound

Ultrasound scanning has quickly become an important diagnostic tool in dermatology due to its cost effectiveness, ease of use and safe noninvasive method of demonstrating small differences between nevi and melanoma. Ultrasound proves useful in preoperative situations and skin therapy monitoring because it can provide information about inflammatory processes of skin and subcutaneous tissue as well as axial and lateral extension of tumors [47, 48]. In dermatology, there are two types of probes used: electronic 7.5 to 13 MHz linear probes and sectorial mechanical 10 to 20 MHz probes [49, 50]. 20 kHz represents the upper frequency limit of human hearing and therefore using the 7.5 to 20 MHz probe is very safe for imaging techniques [51].

Table 2. Resolution of high frequency transducers [53]

Frequency (MHz)	Axial resolution (m)	Lateral resolution (m)	Penetration (mm)
7.5	200	400	>15
10	150	300	>15
20	100	350	7
40	30	94	4
50	39	120	4
100	11	30	2

Transducers with higher frequency wavelengths are beneficial for diagnosing skin lesions because they allow better resolution of small lesions located near the skin surface. However, with increasing frequency, the depth of penetration of ultrasound waves decreases (*i.e.* 20 MHz ultrasound penetrates only 8 mm), leaving the choice of the probe frequency dependent on the diameter and site of the lesion [51, 52]. Electronic 7.5 to 13 MHz linear probes depict flat and regular surfaces effectively and provide a wider field of surface vision and, therefore, a wider view than sectorial probes. Water bath sectorial probes with 10 to 20 MHz frequency have very superficial focusing and are excellent to study irregular surfaces. While various ultrasound transducers examine up to depths of 1.5 cm or more, 20 MHz probes have been effective at assessing the depth of melanoma invasion and 100 MHz probes have been useful for determining tumor thickness of thin melanocytic skin lesions *(table 2*, *figure 3)* [49, 50, 53, 54].

Resolution of ultrasound systems can refer to either axial or lateral resolution. The axial resolution is the smallest thickness that can be measured and the lateral resolution refers to the width of the smallest structures that can be resolved [51]. In general, ultrasound systems convert the voltage changes recorded by the transducer and display these signals as images. There are different types of signal processing ranging from A through E [53]. B-scans combine the information from sequential A-scans (Acoustic scan) and display each point according to its relative brightness (hence B-scan). Each point on a B-scan is brighter or darker, corresponding to the intensity of echoes from the corresponding anatomic structure. Therefore, B-scans provide images that resemble anatomic cross sections of scanned tissues [55]. Currently, B-scans are mainly used as ultrasonographic procedures in dermatology using intermediate- or high-frequency ultrasound systems while A-scan ultrasound systems are mainly used in ophthalmology. However, A scans can be used to assess skin thickness and C, D, and E-scans are various forms of B-scan addition also useful in dermatology *(figure 4)* [53].

With sonography, the preoperative tumor thickness is sometimes overestimated because of an underlying inflammatory infiltrate, which is also visualized as a hypoechoic area and cannot be distinguished from melanoma [51]. The dermatologic applications of B-scan ultrasound with 7.5 to 10.0 MHz transducers include the identification and description of suspicious palpable structures within the subcutaneous (solid, cystic, and complex); exploration of deeper aspects of larger tumors, assessing the relationship to nerves and vessels to provide crucial preoperative information; and follow-up of patients with malignant skin tumors including melanomas [56]. According to various studies, 7.5 to 10 MHz ultrasound transducers have excel-

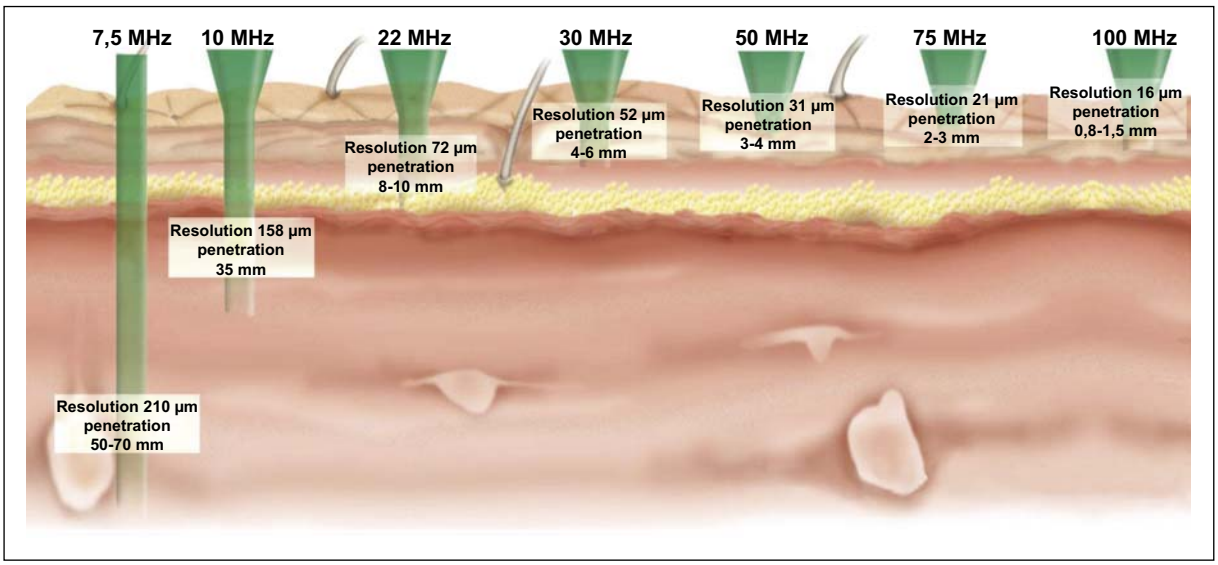

Figure 3. A, B) Sonograpy frequency resolutions (Used with permission of Taberna Pro Medicum, Lüneburg, Germany).

lent sensitivity (99.2%) and specificity (99.7%) [51, 57-59]. However, in patients with melanoma, ultrasound scanning should be performed every 3 to 12 months according to the thickness of the primary melanoma [57-60]. Despite various frequency transducers examining depths greater than 1.5 cm, melanoma metastasis cannot be separated from that of another tumor. The quality of information depends heavily on the skill and experience of the examiner, clinical setting and history of melanoma. Ultrasound systems available for dermatological examinations are the Dermascan C (Cortex Technology, Hadsund, Denmark) *(figures 5A-B)*, DUB 20 (Taberna pro medicum, Lüneburg, Germany) *(figure 6)*, SSA-340 A (Toshiba Medical Systems, Neuss, Germany), and the Siemens Sonoline Elegra (Siemens, Erlangen, Germany), AU 4 Idea, and AU 5 Idea sonography (Esaote Biomedica, Genoa, Italy) *(figures 7A-B)*.

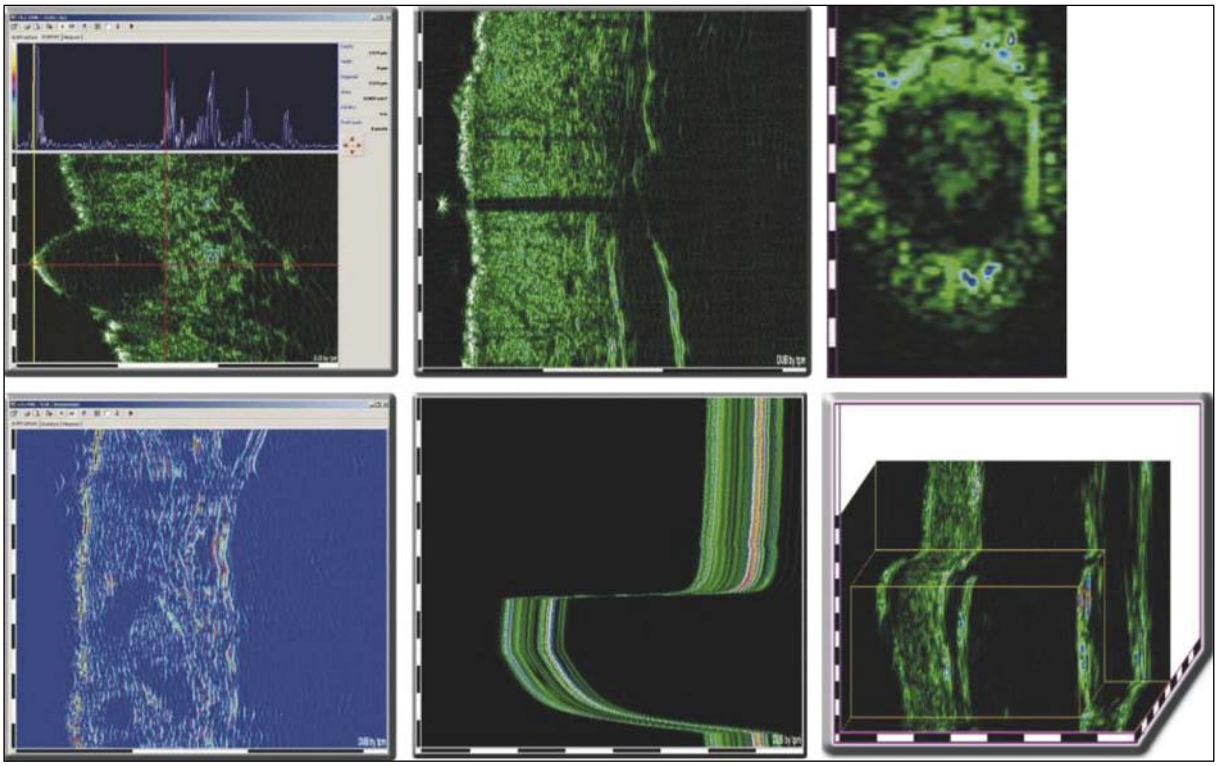

Figure 4. Different types of ultrasonographic signal processing. Top (left to right): A-Scan, B-Scan (built up from 384 high frequency A-Scans), C-Mode (3D scan in horizontal cuts in different vertical layers [depth]), Bottom (left to right): RF-Scan (Raw data behind the recorded image), M-Scan (Skin elasticity measurement with high frequency digital ultrasound with a Vacuum Elasto Pump), 3D-Scan (From 10-30 parallel B-Scans). (Used with permission of Taberna Pro Medicum, Lüneburg, Germany).

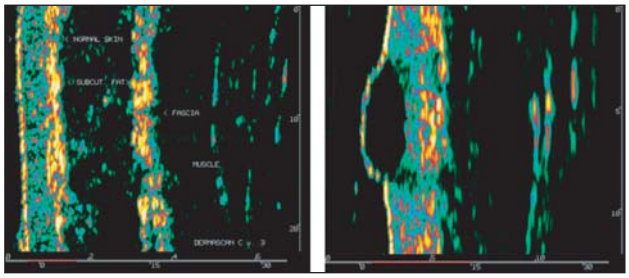

Figure 5. Images aquired with the Dermascan C system (Used with permission of Cortex Technology, Hadsund, Denmark). **A)** Normal forearm. **B)** Melanoma.

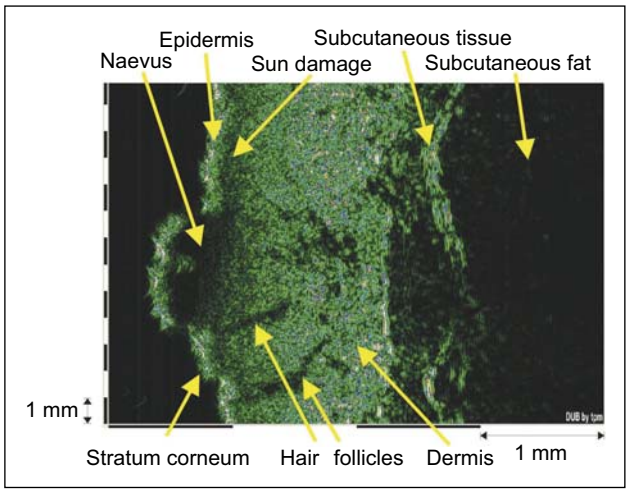

Figure 6. Pigmented lesion analyzed with DUB system 75 MHz (Used with permission of Taberna Pro Medicum, Lüneburg, Germany).

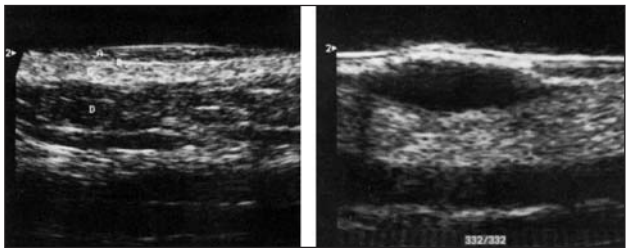

Figure 7. Images acquired on an Esaote AU5 ultrasound system, using a SMA50 probe. (Cortesy of Teresa Cammarota, Director of Radiology, Azienda Ospedaliero-Universitaria S.Giovanni Battista di Torino, Italy.). **A)** (Left): Normal skin, of abdominal wall. (20 MHz): A gel; B entrance echo; C dermis; D subcutaneous tissue. **B)** (Right): Melanoma, 2.43 mm thick (20 MHz): The neoplasia presents sharp edges and an intensely hypoechogenic and homogeneous pattern and is infiltrating the superficial dermis.

Laser based technology

Optical Spectroscopy (CSLM – Confocal scanning laser microscopy) is an efficient *in vivo* imaging tool that allows for *in vivo* examination of the epidermis and papillary dermis, which is equivalent to the resolution of conventional microscopes. Assessment of a PSL by CSLM relies on the interpretation of images of micro-anatomical structures, which resembles a histopathological evaluation with similar criteria [61]. In CSLM, a laser beam is passed through a light source aperture and focused by an objective lens into a small focal volume within a fluorescent specimen. A mixture of emitted fluorescent light as well as reflected laser light from the illuminated spot is then recollected by the objective lens. A beam splitter separates the light mixture by allowing only the laser light to pass through while reflecting the fluorescent light onto a detection apparatus with a pinhole-sized spatial filter. The florescent light passes through the pinhole allowing for detection by a photomultiplier tube or avalanche photodiode, which transforms the light into an electrical signal recorded by the computer. Images of horizontal sections are reconstructed into three-dimensions using multiple tomograms in the horizontal direction [62]. CSLMcan obtain lateral resolutions up to 0.5-1.0 µm and axial resolutions (section thickness) up to 3-5 µm with longer wavelengths of light allowing for measurements of greater depth up to the papillary dermis [63]. Newer CSLM techniques use fiber-optic imaging instead of the pinhole aperture detector which allows for more flexible handheld devices for *in vivo* clinical use [64, 65]. *In vivo* CSLM is capable of identifying distinct patterns and cytologic features of benign and malignant PSLs which correlate with the histological criteria for melanoma *(table 3*, *figure 8)* [61, 66, 67]. Currently, two forms of CSLM application have been established in dermatology: the reflectance mode in the clinical field and the fluorescence mode in research. The reflectance mode demonstrates naturally occurring tissue components, whereas the fluorescent CSLM achieves contrast by the dynamic distribution pattern of the dye emission [68].

Reflectance CSLM depends on the inherent reflective properties of tissue structures and the presence of melanin, which results in a bright-white image signal that illuminates the cytoplasm of melanin-containing cells like pigmented keratinocytes, melanocytes, and melanophages [69]. Free cytoplasmic melanin pigments and cytoplasmic pigmented and nonpigmented melanosomes provide strong contrast for infrared laser light resulting in bright cytoplasm [66, 69-71]. Using near infrared illumination, the maximum depth of imaging is limited by the scattering of the sc surface and the optics of the skin [72]. There are two types of reflectance CSLM, diffuse and polarized.

Diffuse reflectance spectroscopy in the wavelength range of 550 to 1,000 nm has oblique incidence imaging which helps to distinguish between benign and cancer-prone skin lesions [73, 74]. Polarized reflectance spectroscopy provides real-time diagnostically useful information for precancerous lesions which are characterized by increased nuclear size, increased nuclear/cytoplasmic ratio, hyperchromasia and pleomorphism, which are currently assessed by invasive biopsies [75, 76]. Pellacani *et al.* found the presence of non-edged dermal papillae, atypical cells, and isolated nucleated cells within dermal papilla, pagetoid cells, widespread pagetoid infiltration, and cerebriform clusters to be strongly correlated with MM diagnosis in their reflectance CSLM examination [77, 78].

Fluorescence CSLM depends on different fluorescent molecules (endogenous or exogenous) emitting florescence at different levels in tissue. Accordingly, a laser light with the appropriate wavelength can be used to excite these fluores-

Table 3. Key features of pigmented lesions by CSLM [66]

	Nevus	Dysplastic nevus	Melanoma
Cytology	Round-oval, bright, monomorphic Nevus cell nests	Round-oval, bright, larger cells present Nevus cell nests	Bright, polymorphous cells, occasional, irregular (star) shaped morphology Nesting poorly defined
Brightness of image	Individual cells appear bright	Individual cells appear bright; focal, small, bright refractile granules; focal grainy image	Scattered bright, refractile granules, indistinct grainy/hazy image; intracellular and extracellular location
Dendrites	±; when present, small simple branching pattern	±; when present, small simple branching pattern	Frequent, large, complex branching pattern
Keratinocyte cell border	Readily detected	Focal absence	Poorly defined

±, Present or absent.

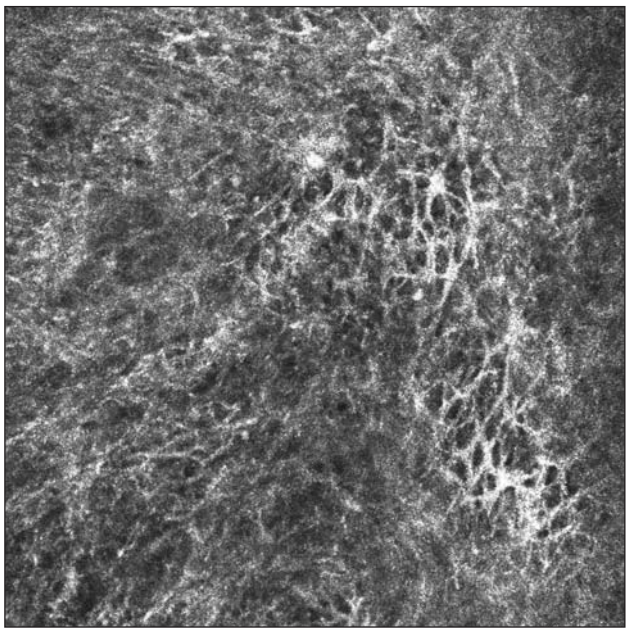

Figure 8. Melanoma on sun damaged skin acquired with Confocal Laser-Scanning Microscopy. Sheets of spindle cells in the superficial dermis can be observed. x: –0.74 mm, y: 2.24 mm, z: –59.88 um, Laser Power: 2.1 mW (Cortesy of Dr. Harold S. Rabinovitz, Voluntary Professor, Department of Dermatology and Cutaneous Surgery, Miller School of Medicine, Miami, Florida, USA).

cent molecules to emit a long wavelength signal which can be detected and displayed on a grey scale [79]. Anikijenko *et al.* showed that fluorescent labeled antibodies injected in an animal melanoma model showed a pathological overexpression of protein and also changes in the microvascular structures that enabled *in vivo* detection of melanoma and surrounding blood vessels in athymic mice [80].

Remarkably, the presence or absence of monomorphic melanocytes as a single diagnostic criterion has been found to have a sensitivity up to 98.2% and a specificity up to 98.9% *(table 4)*. However, in its current state of technological development, CSLM has two major limitations compared with conventional histology. It has a poor resolution of chromatin patterns, nuclear contours and nucleoli and can assess micro-anatomical structures only to a depth of approximately 300 µm [63]. Thus, processes in the reticular dermis cannot be examined for the presence or absence of invasion. Furthermore, melanomas without an intradermal component will most likely escape detection by CSLM in its current state [61]. The main advantage of CSLM is that it permits non-invasive quasi-histological assessment of the skin 'at the bedside'. Multiple sites and lesions can be examined during the same visit, the same lesion can be evaluated at different time points, and images are available immediately for electronic storage and histopathology consultation [61]. Various CSLMs on the market use the technology described above, including Vivascope® 1500 and 3000 (Lucid Inc, NY USA), and Optiscan™ (Optiscan Pvt Ltd, Australia). Lucid, Inc. (www.lucid-tech.com) developed the VivaNet® telemedicine server and network which is designed to transfer and manage clinical data between dermatology practitioners using VivaScope® Confocal imagers with pathologists or other medical specialists.

Optical coherence tomography (OCT) was developed in the late 1980s. While this technique was originally used to examine eye structure, it is now used widely in dermatology [81]. OCT is analogous to ultrasound B-mode imaging with the exception that it uses light rather than sound waves [82, 83]. OCT is described as an intermediate imaging device between ultrasound and CSLM that produces high resolution cross-sectional images of the internal microstructure of living tissue resembling an unstained histopathological section of skin [84, 85]. In contrast to the eye, which is naturally a low light scattering transparent medium, the skin is nearly non-transparent due to absorption and scat-

Table 4. Sensitiviy and Specificity observed in various clinical trials done with VivaScope® 1500 and the VivaScope® 3000

Investigator	Year	Cases	Sensitivity	Specificity	Accuracy
Gerger, *et al.* [158]	2004	117 (27 MM)	98.2%	98.9%	98.7%*
Pellacani, *et al.* [78]	2005	102 (37 MM)	97.3%	72.3%	81.3%
Gerger, *et al.* [159]	2006	162 (27 MM)	90.7%	98.9%	96.3%**
Pellacani, *et al.* [77]	2007	351 (136 MM)	91.9%	69.3%	78.1%

**Diagnostic criteria – monomorphic melanocytes only.*

***Accuracy for melanoma.*

tering; the former is mainly influenced by the concentration of melanin and hemoglobin, while the latter, by differences in the refraction index. In the wavelength range of 700 to 1,300 nm, absorption is relatively low, so that light penetrates deep into the skin and optical inhomogeneities are the main factor influencing the image [81]. When illuminating the skin, most of the photons are scattered more than once, which can lead to artifacts in the image. In the skin and other highly scattering tissues, OCT can image small blood vessels and other structures as deep as 1-2 mm beneath the surface [86, 87].

The OCT technique is based on the wave principles of the Michelson interferometer. The light sources used for OCT are low coherent superluminescent diodes operating at a wavelength of about 810 nm to 1,300 nm. OCT provides *in vivo* two-dimensional images with a scan length of a few millimeters, a resolution of about 15 µm and a maximum detection depth of 1.5-2 mm [72, 81, 86, 87]. OCT with an 810 nm light source is able to examine skin depths up to 700 µm while a 1,313 nm light source can examine up to 1.2-2 mm with reduced scattering [86, 87]. The reflection of the skin surface can be reduced by application of an ointment or glycerol, which makes the skin more transparent, reduces light scattering and increases detection depth [81, 88]. Alternatively, short coherence length can be achieved by ultrasound femtosecond laser pulses which can travel two paths [83, 89]. The first light path travels through air and is reflected back by a mirror and the second focuses directly into the skin. These two reflected lights combine at the detector. When the optical paths of the two beams are equal, the light from the two beams interferes constructively giving a bright spot, whereas when they are out of phase, they interfere destructively. Images are logarithmic false color or grey scale and are obtained by scanning the mirror at the end of the light path and the incident spot. Even though it is possible to almost achieve real-time imaging, the resolution only enables the visualization of architectural changes and not of single cells [81]. Axial resolution depends on the coherence length of the light source, whereas the lateral resolution is given by the focal spot size and the scan step. A calculation of the thickness of layers, the intensity of the signal and the light attenuation coefficient in different depths can be performed on the averaged A-scan in a region of interest. Melanocytic skin tumors show increased light scattering and more homogenous signal distribution than healthy skin. The disappearance of the second intensity peak, which represents an intact border between the epidermis and dermis, is suggestive for infiltrative malignant melanoma (MM) [81].

OCT measurement is unobtrusive, safe, and has no side effects. Because of the fast scanning mode (4 s for 4 mm scan length) and the low output power of the light source (in a range of a few milliwatts), this technique meets the safety standards for irradiation of tissue [81]. Compared to other non-invasive methods, OCT has higher resolution than ultrasound and greater detection depth and image size than CSLM [90]. Newer OCT modalities, such as the Dopppler OCT, spectroscopic (absorption) and wavelength-dependent OCT, and OCT elastography are more precise and accurate with more real-time images [91]. A portable fiber-optic based OCT requires only 1 second to simultaneously provide high-resolution images of skin structure, collagen birefringence and blood flow [92]. With the Doppler and phase-resolved techniques, one can visualize the location of vessels and capillaries as well as determine the flow velocity in PSLs [93, 94]. Newer systems allow the storage of data and images in a digital format that enables quantitative software analysis of images.

Laser Doppler perfusion imaging (LDPI)

The vascularization of melanoma lesions has been a primary interest for many researchers. Microcirculatory activity within a tumor is believed to reflect focal changes within the boundaries of the lesion itself, irrespective of anatomical localization and even of the species of the host [95]. MMs usually show a higher heterogeneity in their structure and a higher vessel density when compared to benign PSLs because of neovascularization which starts very early during the radial growth phase [96-98]. Barnhill *et al.* suggested that, in terms of vessel counts, vascularization gradually increases during the transition process from benign nevi to dysplastic nevi and finally primary melanomas [96]. Furthermore, Tur *et al.* and Fallowfield *et al.* described the excess of pronounced vasculature as an indication that a nevi has a high chance of malignancy [95, 99]. Accordingly, vascularization is gaining importance in the assessment of PSLs and has potential as an adjunct to clinical diagnosis and follow-up. Histopathologically MMs are more highly vascularized than benign nevi and various studies have demonstrated the intimate relationship between vascularization and the degree/level of skin blood flow in blood perfusion techniques [96, 98, 100-103]. Laser Doppler perfusion monitoring (LDPM) as well as LDPI both demonstrate significant, although not completely discriminative, differences in perfusion levels between MM and benign PSLs [104].

The principle behind LDPI is the doppler effect on monochromatic radiation caused by movement of erythrocytes in the microvascular network [105]. The output of the LDPI system consists of two different two-dimensional data sets, perfusion and total backscattered light intensity (TLI), with a point-to-point correspondence. The blood perfusion data set, represented by a color-coded image, is calculated from the backscattered and Doppler-shifted light, defined as the product of the red blood cells mean velocity times their concentration in the sampled tissue volume [103]. The second data set maps the TLI and is coded into a photographic-like grey scale image of the lesion. When the laser beam is reflected by the erythrocytes, the returning signal is recorded in the head of the scanner and translated into an electrical impulse; a scale of six colors demonstrates increasing degrees of perfusion in colors of blue, green, yellow and red [105]. Since laser light is the origin of this type of image, it should not be confused with common optical grey scale images generated by broadband backscattered light. Each recorded image consists of 64 × 64 measurement sites and represents the blood perfusion in a skin area of approximately 13 × 13 mm. LDPI is influenced by the number and the velocity of erythrocytes in the tissue [106]. Several studies showed that LDPI has a sensitivity of almost 100% and a specificity of 85-90% [104, 107]. Stucker *et al.* examined 189 patients with LDPI and found that perfusion was 3.6 ± 1.5 times higher in MMs and 2.2 ± 1.1 higher in suspicious melanocytic nevi than in healthy skin [104]. MMs were found to have a significantly higher flow than clinically suspicious melanocytic nevi ($p < 0.001$) and at least 1.8 times higher flow values than

normal healthy skin [104]. Cutaneous blood flow measurement can play an important part in the assessment of melanoma and can possibly be used as an adjunct to clinical diagnosis and follow-up, and as a source of valuable preoperative information about tumor vascularization [104, 107, 108].

Other imaging

Electrical bio-impedance

Several researchers have used electrical bio-impedance to assess skin cancers and other cutaneous lesions [109-113]. Electrical impedance of tissue reflects transient and special physical properties based on specific frequency regions and dispersion [114, 115]. β-dispersion (kilohertz to hundreds of megahertz) is an electrical bio-impedance mainly affected by the shape of the cells, structure of cell membranes and amount of water (both intra- and extracellular). Based on these features, electrical impedance of cancer cells and healthy cells are different because cancer cells have a different shape, size and orientation – the same criteria as used in histopathological evaluation [110-113].

Measurements of suspicious PSLs are made with an electrical impedance spectrometer both over the center of the lesion as well as an ipsilateral reference skin site. Prior to measurements, the site and lesion are soaked with 0.9% normal saline solution (pH 6) for 1 min to reduce the naturally high impedance of the SC and increase the contact between the tissue and probe. Magnitudes between 1 and 10 kHz and phases between 0.1 and 1 MHz are used to differentiate melanoma from benign nevi [109]. Impedance spectra of the lesions and the reference skin are measured at five depth levels, approximately 0.1-2 mm into the tissue [109, 116]. Newer models of electrical impedance have a digital camera along with an automated software analysis. The induced electric current is detected at each sensor element and measured using a trans-impedance technique, while the other electrodes remain at ground potential [117]. The typical amplitude applied between the source electrode and the measuring probe is in the range of 2.5 V with a frequency range of 100 Hz-100 kHz. After the probe is applied to the lesion, the measured trans-impedance signals are converted to digital signals and transferred to the computer for further analysis [116]. A digital picture of the lesion and its surroundings is recorded followed by a close-up frame of the lesion. The borders and axes of the lesion are displayed on the computer and an automatic algorithm provides five parameters to describe the lesion. The first parameter is asymmetry (A1 and A2) which is defined as the ratio between the non overlapping area of the lesion when folded over either of the two perpendicular axes, and the total area. The ratio between the squared perimeter of the lesion and a factor of the area inside the border is defined as the second border parameter (B). The color parameter (C) is defined as the standard deviation of the red-gray levels inside the border. Finally, the surface (S) is defined as the area of the lesion in square millimeters [116]. The combined examination of electrical impedance scanning and image analysis lasts approximately 7 minutes [116].

Electrical impedance has a high sensitivity of almost 100 percent for *in situ* and thin melanomas [116]. Therefore, electrical impedance can differentiate melanoma from benign nevi with studies demonstrating ranges of 92-100% sensitivity and 67-75% specificity [109, 117]. However, electrical impedance properties of human skin vary significantly with the body location, age, gender, and season [118-121]. Aberg *et al.* studied the bio-electrical impedance spectra from skin cancer and other lesions by using both regular non-invasive probes and a novel micro-invasive electrode system with a surface furnished with tiny spikes that penetrate the SC [122]. Even though the spiked electrode is invasive by definition, Aberg *et al.* considered it micro-invasive because the spikes penetrate the SC and epidermis but do not reach the depths of blood vessels or sensory nerves in dermis [122]. Thus, the information from micro-invasive impedance is better suited for detecting subtle skin alterations that manifest beneath the SC, such as melanoma. Aberg *et al.* found that the spiked micro-invasive electrodes are better for melanoma detection (92% sensitivity and 80% specificity) than the regular non-invasive probes [122]. Commonly used instruments in electrical impedance studies include the SciBase II impedance spectrometer (SciBase AB, Huddinge, Sweden), and the TS2000M (Mirabel Medical System Ltd., Migdal Ha'Emek, Israel).

Magnetic Resonance Imaging (MRI)

Recently, MRI has been used for investigating PSLs including melanocytic skin lesions [123-125]. MRI scans utilize radio waves and strong magnets instead of X-rays. The principle behind MRI is the absorption and re-emission of radio waves from tissue protons exposed to a strong magnetic field. Under the influence of radio frequency pulses, a proton returns to a stable low-energy state and emits radio waves that are detected by the coil [126]. A computer translates the pattern of radio waves emitted by the examined tissues into a detailed image. It provides cross-sectional slices of the body as well as parallel slices along the length of the body. Although rarely used, a contrast material may be injected as with CT scans. Differences in MRI signal intensity from structures allow good tissue contrast with T1- and T2- weighted imaging differing in signal contrast characteristics. The spatial resolution produced by conventional MRI machines has been of the order of 1 mm, which has been inadequate for visualizing the different layers of skin that require a resolution of <100 µm. Recently, specific imaging devices have been developed that allow high-resolution MRI imaging of the skin, permitting clear differentiation of the SC, epidermis and dermis *in vivo* with an image acquisition time of 3 minutes 25 seconds and a section thickness of 1.2 mm. With this spatial resolution, the epidermis appears as a high-intensity layer, while dermis appears as hypointense with an irregular interface of subdermal fat [127, 128]. Specialized MRI surface coils have higher resolution than standard coils and are good for dermatologic conditions [129]. In MRI, edema of the surrounding soft tissue and non-homogeneity are features suggesting malignancy [130]. Takahashi *et al.* found that, even though the morphologic features of melanoma obtained by MRI are not helpful for diagnosis, the signal intensity assessed by the tumor-to-fat contrast ratio on T2-weighted images clearly differentiated between melanoma and benign PSLs [131]. Maurer J *et al.* studied 27 melanocytic nevi and 18 MMs with high resolution MRI and determined the signal intensities and signal-to-noise ratios (SNR) and contrast-to-noise ratios (CNR) of tumors in enhanced (T1, T2, water-suppression, and fat-suppression sequences) and contrast-enhanced images (T1

Table 5. Detection of melanoma using FDG-PET

Reference	Year	Metastases	Patients	Sensitivity (%)	Specificity (%)
Gritters *et al.* [160]	1993	All foci*	12	92	100
Steinert *et al.* [161]	1995	All foci	33	92	100
Boni *et al.* [162]	1995	All foci	15	91	67
Blessing *et al.* [163]	1995	Lymph nodes	20	74	93
Wagner *et al.* [164]	1997	Lymph nodes	11	100	100
Macfarlane *et al.* [165]	1998	Lymph nodes	23	85	91
Rinne *et al.* [166]	1998	Skin	100	91	94
Holder *et al.* [167]	1998	All foci	76	94	83
Eigtved *et al.* [168]	2000	All foci	38	97	56
Acland *et al.* [169]	2000	Skin	54	78	87
Swetter *et al.* [170]	2002	All foci	104	84	97
Gulec *et al.* [171]	2003	> 1-cm lesions	29	100	75
		< 1-cm lesions	20	13	33
Mottaghy *et al.* [172]	2007	All foci	127	86	94

**All foci include skin, lymph nodes, liver, lung, neck, scalp, eyelid, and abdomen.*

and fat-suppression sequences). MMs had a higher SNR than melanocytic nevi and a higher CNR than benign lesions [132]. There are some disadvantages with MRI scanning, including its cost, size, duration of evaluation time, and need for specialized training. Additionally, it is not suitable to place patients with metal implants in the tube-shaped apparatus because of the strong magnetic field generated by the cylindrical magnet.

Positron emission computed tomography (PET)

PET is a non-invasive, high-resolution imaging technique used to detect metastatic spread of melanoma earlier than conventional methods. Over seven decades ago, the biochemist Otto Warburg observed that most tumors relied on anaerobic glycolysis even in the presence of abundant oxygen, a phenomenon now known as the "Warburg effect" [133, 134]. Tumor cells are notorious for their consumption of glucose, which is used to sustain their higher proliferative rate and increased need for macromolecular synthesis in comparison to normal healthy cells. 2-deoxyglucose (2-DG) has a structure similar to glucose and its accumulation via upregulated GLUT1 glucose membrane transporters is responsible for increased glucose consumption in tumor cells. Therefore, when 2-DG is labeled with 18-Fluroscence (18F-DG), tumor cells can be detected with imaging techniques [135]. GLUT1 is also considered an early marker for malignancy along with other intracellular enzymes (*i.e.* hexokinase, phosphofructokinase and pyruvate dehdrogenase) that have an increased activity in the metabolic pathways of malignant cells [133-135].

PET using 18F-FDG has been studied extensively since 1991 and shows great promise in the detection of metastatic cutaneous melanoma and may also prove useful in the secondary prevention of primary melanoma in those individuals at high risk or with a familial disposition [136]. Although rare, primary melanomas have also been found in ocular, gastrointestinal, anorectal, genitourinary, mucosal, leptomeningeal, sinonasal, pulmonary, mediastinal, ovarian, vaginal, and vulvar sites and can represent diagnostic challenges [137-148]. PET may be valuable in detecting these primary melanocytic lesions in non-skin sites as a dermatologist's trained eye and the other diagnostic techniques described above can only detect those primary melanomas localized to skin.

When 18F-FDG is used, it emits a positron which is directed onto negatively charged electrons. When the two particles collide and exterminate each other at 180°, two photons are formed, with each having an energy of 511 KeV [149]. PET scan has the ability to detect these photons, localize their source of origin, and produce an image based on the photon activity. The entire body can be analyzed either in qualitative or quantitative measurements, which may be helpful in differentiating between benign and malignant cells and determining the treatment response [150-155]. *Table 5* displays the overall sensitivity and specificity of PET in different studies. When compared to ultrasound, PET scan is more costly and time consuming. However, ultrasound examination of lymph node metastasis requires more time due to the sequential examination of individual lymph nodes. Additionally, whole-body PET scanning is cheaper than whole-body MRI scanning [156, 157]. The sensitivity of PET is also decreased when tumor size is small *(table 6)*.

Conclusion

The timely diagnosis and management of melanoma during its early stages is critical for a patient's extended survival. As mentioned, numerous non-invasive imaging methods are currently available for patients who are diagnosed with or at risk for melanoma like the dermoscopes, MoleMax™, SIAscope™, SolarScan®, MelaFind™, Ultrasonography, MRI and PET scan; LASER based technology like CSLM, OCT, LDPI and electrical bio-impedance. The major disadvantages for non-invasive testing are the cost and patient anxiety. Therefore, it is critical to consider which imaging methods are useful and feasible. In the clinical setting, computer-based systems like MelaFind™ and SolarScan®, may provide diagnostic information. However some testing devices are not appropriate for the office setting like MRI and PET scans. Apart from the cost and office setting, there are several issues that should be considered before using non-invasive methods for melanoma diagnosis. The most important are the privacy and security of photography and the training and experience of dermatologists and/or physicians. Some other issues for consideration are the number of photographs required, when photographs and procedures

Table 6. Comparison of technologies

Technology	Sensitivity	Specificity	Advantages	Disadvantages
MoleMax	N/A	N/A	Two camera system; no oil immersion required; transparent overlay for follow-up; total body photography	
Spectrophotometric Intracutaneous Analysis (SIAscope)	96% [38] 82.7% [33]	87% [38] 80.1% [33]	Diagnosis of PSLs up to 2 mm; visualizes skin structure, vascular composition and reticular pigment networks; handheld scanner	
SolarScan	91% [24]	68% [24]	Empirical data base for comparison; session and image-level calibration; recorded on graphical map of body; detection of 14 shades of dermatoscopic colors, including Blue-White veil	Requires oil immersion
MelaFindTM	95-100% [34, 35]	70-85% [34, 35]	Multispectral sequence of images created in < 3 s; images have > 1 million pixels	
DermDOCTM	N/A	N/A	High quality images; variable magnification; macro/micro application	Loses image resolution after conversion of video to images
Tape Stripping mRNA	68.7% [44]	74.5% [44]	Rapid and easy to perform; painless; practical for any skin surface; can retest same lesion	Need larger gene expression profiles for comparison
Ultrasound Technology	99.2% [51, 57-59]	99.7% [51, 57-59]	Cost effective; information about inflammatory processes of skin in relationship to nerves and vessels	Depth of penetration decreases with increasing frequency; tumor thickness may be overestimated due to underlying inflammatory infiltrate; melanoma metastasis cannot be separated from that of another tumor
Confocal scanning laser microscopy (CSLM)	98.15% [158]	98.89% [158]	Histopathological evaluation at bedside with similar criteria; longer wavelengths can measure up to papillary dermis; fiber-optic imaging allows for flexible handheld devices	Poor resolution of chromatin patterns, nuclear contours and nucleoli; assesses micro-anatomical structures only to depth of 300 μm; melanomas without *in situ* component will likely escape detection
Optical Coherence Tomography (OCT)	N/A	N/A	High resolution cross-sectional images resembling histopathological section of skin; 4 mm scan length obtained in 4 s; higher resolution than ultrasound and greater detection depth than CSLM; Doppler and phase-resolved techniques allow visualization of vessels and determination of flow velocity	Photons are scattered more than once, which can lead to image artifacts; ointment or glycerol may be needed to reduce scattering and increase detection depth; visualization of architectural changes and not single cells
Laser Doppler Perfusion Imaging (LDPI)	~100% [104, 107],	85-90% [104, 107],	Adjunct to clinical diagnosis and follow-up; source of preoperative tumor vascularization	Differences in perfusion levels between MM and benign PSLs are not completely discriminative
Electrical Bio-impedance	92-100% [109, 117]; spiked micro-invasive electrodes: 92% [122]	67-75% [109, 117]; spiked micro-invasive electrodes: 80% [122]	Complete examination lasts 7 min.	Must be soaked with 0.9% normal saline solution (pH 6) for 1 min to reduce impedance of the SC; electrical impedance properties of human skin vary significantly with the body location, age, gender, and season
Magnetic Resonant Imaging (MRI)	N/A	N/A	Permits clear differentiation of the SC, epidermis and dermis *in vivo*	Cost; equipment size; acquisition time; need for specialized training; contraindicated in patients with metal implants
Positron Emission Computer Tomography (PET)	See *table 5*	See *table 5*	Detects micro metastasis based on abnormal cellular metabolic activity; may be valuable in detecting primary melanocytic lesions in non-skin sites; whole-body PET scanning is cheaper than whole-body MRI	More costly and time consuming than ultrasound; sensitivity decreases when tumor size is small

should be repeated, and how the cost of photography will be reimbursed by insurance companies and Medicare. We suggest all PSLs should be evaluated clinically but those that are suspicious or do not conform completely to the ABCD criteria may need further in depth evaluation by any of the non-invasive techniques. All suspicious lesions should be followed up within 3-6 months. Even though digital technology has an increasingly important role in the diagnosis of melanoma, there is no substitute for the trained human eye and hands-on clinical experience. ■

Conflict of interest: Jitendrakumar K. Patel and Sadegh Amini were previously involved in a study sponsored by Electro-Optical Sciences, Inc. as research fellows at the University of Miami Miller School of Medicine. Brian Berman was the principal investigator of the study by Electro-Optical Sciences, Inc. at the University of Miami Miller School of Medicine. All other authors have no conflict of interest.

References

1. Balch CM, Buzaid AC, Soong SJ, *et al*. Final version of the american joint committee on cancer staging system for cutaneous melanoma. *J Clin Oncol* 2001; 19: 3635-48.
2. Wolf IH, Smolle J, Soyer HP, Kerl H. Sensitivity in the clinical diagnosis of malignant melanoma. *Melanoma Res* 1998; 8: 425-9.
3. Curley RK, Cook MG, Fallowfield ME, Marsden RA. Accuracy in clinically evaluating pigmented lesions. *BMJ* 1989; 299: 16-8.
4. Kittler H, Pehamberger H, Wolff K, Binder M. Diagnostic accuracy of dermoscopy. *Lancet Oncol* 2002; 3: 159-65.
5. Ascierto PA, Palmieri G, Celentano E, *et al*. Sensitivity and specificity of epiluminescence microscopy: Evaluation on a sample of 2731 excised cutaneous pigmented lesions. the melanoma cooperative study. *Br J Dermatol* 2000; 142: 893-8.
6. Rubegni P, Cevenini G, Burroni M, *et al*. Automated diagnosis of pigmented skin lesions. *Int J Cancer* 2002; 101: 576-80.
7. Skvara H, Teban L, Fiebiger M, Binder M, Kittler H. Limitations of dermoscopy in the recognition of melanoma. *Arch Dermatol* 2005; 141: 155-60.
8. Pehamberger H, Steiner A, Wolff K. In vivo epiluminescence microscopy of pigmented skin lesions. I. pattern analysis of pigmented skin lesions. *J Am Acad Dermatol* 1987; 17: 571-83.
9. Binder M, Schwarz M, Winkler A, *et al*. Epiluminescence microscopy. A useful tool for the diagnosis of pigmented skin lesions for formally trained dermatologists. *Arch Dermatol* 1995; 131: 286-91.
10. Asawanonda P, Taylor CR. Wood's light in dermatology. *Int J Dermatol* 1999; 38: 801-7.
11. Kopf AW, Salopek TG, Slade J, Marghoob AA, Bart RS. Techniques of cutaneous examination for the detection of skin cancer. *Cancer* 1995; 75: 684-90.
12. Chwirot BW, Chwirot S, Redzinski J, Michniewicz Z. Detection of melanomas by digital imaging of spectrally resolved ultraviolet light-induced autofluorescence of human skin. *Eur J Cancer* 1998; 34: 1730-4.
13. Church J, Williams H. Another sniffer dog for the clinic? *Lancet* 2001; 358: 930.
14. Balseiro SC, Correia HR. Is olfactory detection of human cancer by dogs based on major histocompatibility complex-dependent odour components?–A possible cure and a precocious diagnosis of cancer. *Med Hypotheses* 2006; 66: 270-2.
15. Williams H, Pembroke A. Sniffer dogs in the melanoma clinic? *Lancet* 1989; 1: 734.
16. Offidani A, Simonetti O, Bernardini ML, Alpagut A, Cellini A, Bossi G. General practitioners' accuracy in diagnosing skin cancers. *Dermatology* 2002; 205: 127-30.
17. Fleming MG. Digital dermoscopy. *Dermatol Clin* 2001; 19: 359-67; (ix).
18. Rubegni P, Burroni M, Andreassi A, Fimiani M. The role of dermoscopy and digital dermoscopy analysis in the diagnosis of pigmented skin lesions. *Arch Dermatol* 2005; 141: 1444-6.
19. Roesch A, Burgdorf W, Stolz W, Landthaler M, Vogt T. Dermatoscopy of "dysplastic nevi": A beacon in diagnostic darkness. *Eur J Dermatol* 2006; 16: 479-93.
20. Joel G, Schmid-Saugeon P, Guggisberg D, *et al*. Validation of segmentation techniques for digital dermoscopy. *Skin Res Technol* 2002; 8: 240-9.
21. Rubegni P, Burroni M, Dell'eva G, Andreassi L. Digital dermoscopy analysis for automated diagnosis of pigmented skin lesions. *Clin Dermatol* 2002; 20: 309-12.
22. Schindewolf T, Schiffner R, Stolz W, Albert R, Abmayr W, Harms H. Evaluation of different image acquisition techniques for a computer vision system in the diagnosis of malignant melanoma. *J Am Acad Dermatol* 1994; 31: 33-41.
23. Serup J. High-tech dermatology. *Eur J Dermatol* 2007; 17: 178-80.
24. Menzies SW, Bischof L, Talbot H, *et al*. The performance of SolarScan: An automated dermoscopy image analysis instrument for the diagnosis of primary melanoma. *Arch Dermatol* 2005; 141: 1388-96.
25. Burroni M, Corona R, Dell'Eva G, *et al*. Melanoma computer-aided diagnosis: Reliability and feasibility study. *Clin Cancer Res* 2004; 10: 1881-6.
26. Hoffmann K, Gambichler T, Rick A, *et al*. Diagnostic and neural analysis of skin cancer (DANAOS). A multicentre study for collection and computer-aided analysis of data from pigmented skin lesions using digital dermoscopy. *Br J Dermatol* 2003; 149: 801-9.
27. Lee TK, Claridge E. Predictive power of irregular border shapes for malignant melanomas. *Skin Res Technol* 2005; 11: 1-8.
28. Binder M, Kittler H, Dreiseitl S, Ganster H, Wolff K, Pehamberger H. Computer-aided epiluminescence microscopy of pigmented skin lesions: The value of clinical data for the classification process. *Melanoma Res* 2000; 10: 556-61.
29. Binder M, Steiner A, Schwarz M, Knollmayer S, Wolff K, Pehamberger H. Application of an artificial neural network in epiluminescence microscopy pattern analysis of pigmented skin lesions: A pilot study. *Br J Dermatol* 1994; 130: 460-5.
30. Baxt WG, Shofer FS, Sites FD, Hollander JE. A neural network aid for the early diagnosis of cardiac ischemia in patients presenting to the emergency department with chest pain. *Ann Emerg Med* 2002; 40: 575-83.
31. Itchhaporia D, Snow PB, Almassy RJ, Oetgen WJ. Artificial neural networks: Current status in cardiovascular medicine. *J Am Coll Cardiol* 1996; 28: 515-21.
32. Binder M, Kittler H, Seeber A, Steiner A, Pehamberger H, Wolff K. Epiluminescence microscopy-based classification of pigmented skin lesions using computerized image analysis and an artificial neural network. *Melanoma Res* 1998; 8: 261-6.
33. Moncrieff M, Cotton S, Claridge E, Hall P. Spectrophotometric intracutaneous analysis: A new technique for imaging pigmented skin lesions. *Br J Dermatol* 2002; 146: 448-57.
34. Elbaum M, Kopf AW, Rabinovitz HS, *et al*. Automatic differentiation of melanoma from melanocytic nevi with multispectral digital dermoscopy: A feasibility study. *J Am Acad Dermatol* 2001; 44: 207-18.
35. Gutkowicz-Krusin D, Elbaum M, Jacobs A, *et al*. Precision of automatic measurements of pigmented skin lesion parameters with a MelaFind(TM) multispectral digital dermoscope. *Melanoma Res* 2000; 10: 563-70.
36. DermDOC. Available at: http://www.dermamedicalsystems.com. Accessed oct, 2006.
37. Dermascope. Available at: www.astronclinica.com. Accessed 10/05, 2006.
38. Michalska M, Chodorowska G, Krasowska D. SIAscopy–a new non-invasive technique of melanoma diagnosis. *Ann Univ Mariae Curie Sklodowska [Med]* 2004; 59: 421-31.
39. Menzies SW, Gutenev A, Avramidis M, Batrac A, McCarthy WH. Short-term digital surface microscopic monitoring of atypical or changing melanocytic lesions. *Arch Dermatol* 2001; 137: 1583-9.
40. SolarScan. Available at: www.polartechnics.com.au/index.htm. Accessed 10/10, 2006.
41. Menzies SW. Automated epiluminescence microscopy: Human vs machine in the diagnosis of melanoma. *Arch Dermatol* 1999; 135: 1538-40.
42. Kopf AW, Elbaum M, Provost N. The use of dermoscopy and digital imaging in the diagnosis of cutaneous malignant melanoma. *Skin Res Technol* 1997; 3: 1-7.

43. Morhenn VB, Chang EY, Rheins LA. A noninvasive method for quantifying and distinguishing inflammatory skin reactions. *J Am Acad Dermatol* 1999; 41(5 Pt 1): 687-92.
44. Berardi P, Arcangeli F. The tape stripping toluidine blue (TSTB) method in the diagnosis of malignant melanoma: An investigator-blind study. *Melanoma Res* 1992; 2(2): 93-9.
45. Wachsman W, Zapala M, Udall D, et al. Differentiation of Melanoma from Dysplastic Nevi in Suspicious Pigmented Skin Lesions by Non-invasive Tape Stripping. Available at: http://www.nugeninc.com/pdfs/wachsman_sid_poster_la_2007.pdf. Accessed Aug/25, 2007.
46. Wachsman W, Hata T, Walls L, et al. Development of a multigene classifier to determine the risk of melanoma in suspicious pigmented nevi by non-invasive tape stripping. *International investigative dermatology meeting* 2008.
47. Hoffmann K, Jung J, el Gammal S, Altmeyer P. Malignant melanoma in 20-MHz B scan sonography. *Dermatology* 1992; 185: 49-55.
48. Hoffmann K, el Gammal S, Matthes U, Altmeyer P. Digital 20 mhz sonography of the skin in preoperative diagnosis. *Z Hautkr* 1989; 64: 851-2; (855-8).
49. Rallan D, Dickson M, Bush NL, Harland CC, Mortimer P, Bamber JC. High-resolution ultrasound reflex transmission imaging and digital photography: Potential tools for the quantitative assessment of pigmented lesions. *Skin Res Technol* 2006; 12: 50-9.
50. Moehrle M, Blum A, Rassner G, Juenger M. Lymph node metastases of cutaneous melanoma: Diagnosis by B-scan and color doppler sonography. *J Am Acad Dermatol* 1999; 41: 703-9.
51. Schmid-Wendtner MH, Burgdorf W. Ultrasound scanning in dermatology. *Arch Dermatol* 2005; 141: 217-24.
52. Cammarota T, Pinto F, Magliaro A, Sarno A. Current uses of diagnostic high-frequency US in dermatology. *Eur J Radiol* 1998; 27(Suppl 2): S215-S223.
53. Thiboutot DM. Dermatological Applications of High-Frequency Ultrasound. Available at: http://www.bioe.psu.edu/labs/NIH/derm_app.pdf. Accessed 02/17, 2007.
54. Gambichler T, Moussa G, Bahrenberg K, *et al.* Preoperative ultrasonic assessment of thin melanocytic skin lesions using a 100-MHz ultrasound transducer: A comparative study. *Dermatol Surg* 2007; 33: 818-24.
55. Vassallo P, Wernecke K, Roos N, Peters PE. Differentiation of benign from malignant superficial lymphadenopathy: The role of high-resolution US. *Radiology* 1992; 183: 215-20.
56. Tregnaghi A, De Candia A, Calderone M, *et al.* Ultrasonographic evaluation of superficial lymph node metastases in melanoma. *Eur J Radiol* 1997; 24: 216-21.
57. Blum A, Schlagenhauff B, Stroebel W, Breuninger H, Rassner G, Garbe C. Ultrasound examination of regional lymph nodes significantly improves early detection of locoregional metastases during the follow-up of patients with cutaneous melanoma: Results of a prospective study of 1288 patients. *Cancer* 2000; 88: 2534-9.
58. Voit C, Mayer T, Kron M, *et al.* Efficacy of ultrasound B-scan compared with physical examination in follow-up of melanoma patients. *Cancer* 2001; 91: 2409-16.
59. Schmid-Wendtner MH, Paerschke G, Baumert J, Plewig G, Volkenandt M. Value of ultrasonography compared with physical examination for the detection of locoregional metastases in patients with cutaneous melanoma. *Melanoma Res* 2003; 13: 183-8.
60. Garbe C, Paul A, Kohler-Spath H, *et al.* Prospective evaluation of a follow-up schedule in cutaneous melanoma patients: Recommendations for an effective follow-up strategy. *J Clin Oncol* 2003; 21: 520-9.
61. Busam KJ, Charles C, Lohmann CM, Marghoob A, Goldgeier M, Halpern AC. Detection of intraepidermal malignant melanoma in vivo by confocal scanning laser microscopy. *Melanoma Res* 2002; 12: 349-55.
62. Ono I, Sakemoto A, Ogino J, Kamiya T, Yamashita T, Jimbow K. The real-time, three-dimensional analyses of benign and malignant skin tumors by confocal laser scanning microscopy. *J Dermatol Sci* 2006; 43: 135-41.
63. Rajadhyaksha M, Gonzalez S, Zavislan JM, Anderson RR, Webb RH. In vivo confocal scanning laser microscopy of human skin II: Advances in instrumentation and comparison with histology. *J Invest Dermatol* 1999; 113: 293-303.
64. Delaney PM, King RG, Lambert JR, Harris MR. Fibre optic confocal imaging (FOCI) for subsurface microscopy of the colon in vivo. *J Anat* 1994; 184(Pt 1): 157-60.
65. Delaney PM, Harris MR, King RG. Novel microscopy using fibre optic confocal imaging and its suitability for subsurface blood vessel imaging in vivo. *Clin Exp Pharmacol Physiol* 1993; 20: 197-8.
66. Langley RG, Rajadhyaksha M, Dwyer PJ, Sober AJ, Flotte TJ, Anderson RR. Confocal scanning laser microscopy of benign and malignant melanocytic skin lesions in vivo. *J Am Acad Dermatol* 2001; 45: 365-76.
67. Langley RG, Burton E, Walsh N, Propperova I, Murray SJ. In vivo confocal scanning laser microscopy of benign lentigines: Comparison to conventional histology and in vivo characteristics of lentigo maligna. *J Am Acad Dermatol* 2006; 55: 88-97.
68. Meyer LE, Otberg N, Sterry W, Lademann J. In vivo confocal scanning laser microscopy: Comparison of the reflectance and fluorescence mode by imaging human skin. *J Biomed Opt* 2006; 11; (044012).
69. Busam KJ, Hester K, Charles C, *et al.* Detection of clinically amelanotic malignant melanoma and assessment of its margins by in vivo confocal scanning laser microscopy. *Arch Dermatol* 2001; 137: 923-9.
70. Rajadhyaksha M, Grossman M, Esterowitz D, Webb RH, Anderson RR. In vivo confocal scanning laser microscopy of human skin: Melanin provides strong contrast. *J Invest Dermatol* 1995; 104: 946-52.
71. Langley RG, Rajadhyaksha M, Dwyer PJ, Sober AJ, Flotte TJ, Anderson RR. Confocal scanning laser microscopy of benign and malignant melanocytic skin lesions in vivo. *J Am Acad Dermatol* 2001; 45: 365-76.
72. Kollias N, Stamatas GN. Optical non-invasive approaches to diagnosis of skin diseases. *J Investig Dermatol Symp Proc* 2002; 7: 64-75.
73. Mehrubeoglu M, Kehtarnavaz N, Marquez G, Duvic M, Wang LV. Skin lesion classification using oblique-incidence diffuse reflectance spectroscopic imaging. *Appl Opt* 2002; 41: 182-92.
74. Murphy BW, Webster RJ, Turlach BA, *et al.* Toward the discrimination of early melanoma from common and dysplastic nevus using fiber optic diffuse reflectance spectroscopy. *J Biomed Opt* 2005; 10; (064020).
75. Sokolov K, Nieman LT, Myakov A, Gillenwater A. Polarized reflectance spectroscopy for pre-cancer detection. *Technol Cancer Res Treat* 2004; 3: 1-14.
76. Gurjar RS, Backman V, Perelman LT, *et al.* Imaging human epithelial properties with polarized light-scattering spectroscopy. *Nat Med* 2001; 7: 1245-8.
77. Pellacani G, Guitera P, Longo C, Avramidis M, Seidenari S, Menzies S. The impact of in vivo reflectance confocal microscopy for the diagnostic accuracy of melanoma and equivocal melanocytic lesions. *J Invest Dermatol* 2007; 127: 2759-65.
78. Pellacani G, Cesinaro AM, Seidenari S. Reflectance-mode confocal microscopy of pigmented skin lesions–improvement in melanoma diagnostic specificity. *J Am Acad Dermatol* 2005; 53: 979-85.
79. Delaney PM, Harris MR, King RG. A fibre optic laser scanning confocal microscope suitable for fluorescence imaging. *Opt* 1994; 33: 573-7.
80. Anikijenko P, Vo LT, Murr ER, *et al.* In vivo detection of small subsurface melanomas in athymic mice using noninvasive fiber optic confocal imaging. *J Invest Dermatol* 2001; 117: 1442-8.
81. Welzel J. Optical coherence tomography in dermatology: A review. *Skin Res Technol* 2001; 7: 1-9.
82. Marchesini R, Tomatis S, Bartoli C, *et al.* In vivo spectrophotometric evaluation of neoplastic and non-neoplastic skin pigmented lesions. III. CCD camera-based reflectance imaging. *Photochem Photobiol* 1995; 62: 151-4.
83. Fujimoto JG, Bouma B, Tearney GJ, *et al.* New technology for high-speed and high-resolution optical coherence tomography. *Ann N Y Acad Sci* 1998; 838: 95-107.
84. Huang D, Swanson EA, Lin CP, *et al.* Optical coherence tomography. *Science* 1991; 254: 1178-81.
85. Marchesini R, Bono A, Bartoli C, Lualdi M, Tomatis S, Cascinelli N. Optical imaging and automated melanoma detection: Questions and answers. *Melanoma Res* 2002; 12: 279-86.
86. Schmitt JM, Yadlowsky MJ, Bonner RF. Subsurface imaging of living skin with optical coherence microscopy. *Dermatology* 1995; 191: 93-8.
87. Welzel J, Lankenau E, Birngruber R, Engelhardt R. Optical coherence tomography of the human skin. *J Am Acad Dermatol* 1997; 37: 958-63.
88. Vargas G, Chan EK, Barton JK, Rylander 3rd HG, Welch AJ. Use of an agent to reduce scattering in skin. *Lasers Surg Med* 1999; 24: 133-41.
89. Drexler W, Morgner U, Ghanta RK, Kartner FX, Schuman JS, Fujimoto JG. Ultrahigh-resolution ophthalmic optical coherence tomography. *Nat Med* 2001; 7: 502-7.
90. Veiro JA, Cummins PG. Imaging of skin epidermis from various origins using confocal laser scanning microscopy. *Dermatology* 1994; 189: 16-22.

91. Gambichler T, Moussa G, Sand M, Sand D, Altmeyer P, Hoffmann K. Applications of optical coherence tomography in dermatology. *J Dermatol Sci* 2005; 40: 85-94.
92. Pierce MC, Strasswimmer J, Park BH, Cense B, de Boer JF. Advances in optical coherence tomography imaging for dermatology. *J Invest Dermatol* 2004; 123: 458-63.
93. Zhao Y, Chen Z, Saxer C, Xiang S, de Boer JF, Nelson JS. Phase-resolved optical coherence tomography and optical doppler tomography for imaging blood flow in human skin with fast scanning speed and high velocity sensitivity. *Opt Lett.* Washington DC, USA: Optical Society of America; 2000; 2: 114-116. Available from: http://www.opticsinfobase.org/abstract.cfm?URI=ol-25-2-114. Accessed Feb-20-2007.
94. Chen Z, Milner TE, Wang X, Srinivas S, Nelson JS. Optical doppler tomography: Imaging in vivo blood flow dynamics following pharmacological intervention and photodynamic therapy. *Photochem Photobiol* 1998; 67: 56-60.
95. Fallowfield ME, Cook MG. The vascularity of primary cutaneous melanoma. *J Pathol* 1991; 164: 241-4.
96. Barnhill RL, Fandrey K, Levy MA, Mihm Jr. MC, Hyman B. Angiogenesis and tumor progression of melanoma. quantification of vascularity in melanocytic nevi and cutaneous malignant melanoma. *Lab Invest* 1992; 67: 331-7.
97. Konerding MA, van Ackern C, Steinberg F, Streffer C. Combined morphological approaches in the study of network formation in tumor angiogenesis. *EXS* 1992; 61: 40-58.
98. Ribatti D, Vacca A, Palma W, Lospalluti M, Dammacco F. Angiogenesis during tumor progression in human malignant melanoma. *EXS* 1992; 61: 415-20.
99. Tur E, Brenner S. Cutaneous blood flow measurements for the detection of malignancy in pigmented skin lesions. *Dermatology* 1992; 184: 8-11.
100. Braverman IM, Keh A, Goldminz D. Correlation of laser doppler wave patterns with underlying microvascular anatomy. *J Invest Dermatol* 1990; 95: 283-6.
101. Braverman IM, Schechner JS. Contour mapping of the cutaneous microvasculature by computerized laser doppler velocimetry. *J Invest Dermatol* 1991; 97: 1013-8.
102. Braverman IM, Schechner JS, Silverman DG, Keh-Yen A. Topographic mapping of the cutaneous microcirculation using two outputs of laser-doppler flowmetry: Flux and the concentration of moving blood cells. *Microvasc Res* 1992; 44: 33-48.
103. Wardell K, Braverman IM, Silverman DG, Nilsson GE. Spatial heterogeneity in normal skin perfusion recorded with laser doppler imaging and flowmetry. *Microvasc Res* 1994; 48: 26-38.
104. Stucker M, Esser M, Hoffmann M, *et al.* High-resolution laser doppler perfusion imaging aids in differentiating between benign and malignant melanocytic skin tumours. *Acta Derm Venereol* 2002; 82: 25-9.
105. Stucker M, Horstmann I, Nuchel C, Rochling A, Hoffmann K, Altmeyer P. Blood flow compared in benign melanocytic naevi, malignant melanomas and basal cell carcinomas. *Clin Exp Dermatol* 1999; 24: 107-11.
106. Stucker M, Springer C, Paech V, Hermes N, Hoffmann M, Altmeyer P. Increased laser doppler flow in skin tumors corresponds to elevated vessel density and reactive hyperemia. *Skin Res Technol* 2006; 12: 1-6.
107. Stucker M, Hoffmann M, Memmel U, von Bormann C, Hoffmann K, Altmeyer P. In vivo differentiation of pigmented skin tumors with laser doppler perfusion imaging. *Hautarzt* 2002; 53: 244-9.
108. Ilias MA, Wardell K, Stucker M, Anderson C, Salerud EG. Assessment of pigmented skin lesions in terms of blood perfusion estimates. *Skin Res Technol* 2004; 10: 43-9.
109. Aberg P, Nicander I, Hansson J, Geladi P, Holmgren U, Ollmar S. Skin cancer identification using multifrequency electrical impedance–a potential screening tool. *IEEE Trans Biomed Eng* 2004; 51: 2097-102.
110. Brown BH, Tidy JA, Boston K, Blackett AD, Smallwood RH, Sharp F. Relation between tissue structure and imposed electrical current flow in cervical neoplasia. *Lancet* 2000; 355: 892-5.
111. Zou Y, Guo Z. A review of electrical impedance techniques for breast cancer detection. *Med Eng Phys* 2003; 25: 79-90.
112. Wilkinson BA, Smallwood RH, Keshtar A, Lee JA, Hamdy FC. Electrical impedance spectroscopy and the diagnosis of bladder pathology: A pilot study. *J Urol* 2002; 168: 1563-7.
113. Blad B, Baldetorp B. Impedance spectra of tumour tissue in comparison with normal tissue; a possible clinical application for electrical impedance tomography. *Physiol Meas* 1996; 17(Suppl 4A): A105-A115.
114. Schwan HP. Electrical properties of tissue and cell suspensions. *Adv Biol Med Phys* 1957; 5: 147-209.
115. Foster KR, Schwan HP. Dielectric properties of tissues and biological materials: A critical review. *Crit Rev Biomed Eng* 1989; 17: 25-104.
116. Har-Shai Y, Glickman YA, Siller G, *et al.* Electrical impedance scanning for melanoma diagnosis: A validation study. *Plast Reconstr Surg* 2005; 116: 782-90.
117. Glickman YA, Filo O, David M, *et al.* Electrical impedance scanning: A new approach to skin cancer diagnosis. *Skin Res Technol* 2003; 9: 262-8.
118. Nicander I, Ollmar S. Electrical impedance measurements at different skin sites related to seasonal variations. *Skin Res Technol* 2000; 6: 81-6.
119. Aberg P, Geladi P, Nicander I, Ollmar S. Variation of skin properties within human forearms demonstrated by non-invasive detection and multi-way analysis. *Skin Res Technol* 2002; 8: 194-201.
120. Nicander I, Norlen L, Brockstedt U, Lundh Rozell B, Forslind B, Ollmar S. Electrical impedance and other physical parameters as related to lipid content of human stratum corneum. *Skin Res Technol* 1998; 4: 213-21.
121. Nicander I, Ollmar S, Eek A, Lundh Rozell B, Emtestam L. Correlation of impedance response patterns to histological findings in irritant skin reactions induced by various surfactants. *Br J Dermatol* 1996; 134: 221-8.
122. Aberg P, Geladi P, Nicander I, Hansson J, Holmgren U, Ollmar S. Non-invasive and microinvasive electrical impedance spectra of skin cancer - a comparison between two techniques. *Skin Res Technol* 2005; 11: 281-6.
123. Zemtsov A, Lorig R, Bergfield WF, Bailin PL, Ng TC. Magnetic resonance imaging of cutaneous melanocytic lesions. *J Dermatol Surg Oncol* 1989; 15: 854-8.
124. Zemtsov A, Lorig R, Ng TC, *et al.* Magnetic resonance imaging of cutaneous neoplasms: Clinicopathologic correlation. *J Dermatol Surg Oncol* 1991; 17: 416-22.
125. Takahashi M, Kohda H. Diagnostic utility of magnetic resonance imaging in malignant melanoma. *J Am Acad Dermatol* 1992; 27: 51-4.
126. Caldemeyer KS, Buckwalter KA. The basic principles of computed tomography and magnetic resonance imaging. *J Am Acad Dermatol* 1999; 41: 768-71.
127. Bittoun J, Saint-Jalmes H, Querleux BG, *et al.* In vivo high-resolution MR imaging of the skin in a whole-body system at 1.5 T. *Radiology* 1990; 176: 457-60.
128. Hawnaur JM, Dobson MJ, Zhu XP, Watson Y. Skin: MR imaging findings at middle field strength. *Radiology* 1996; 201: 868-72.
129. Hyde JS, Jesmanowicz A, Kneeland JB. Surface coil for MR imaging of the skin. *Magn Reson Med* 1987; 5: 456-61.
130. Zemtsov A, Lorig R, Bergfield WF, Bailin PL, Ng TC. Magnetic resonance imaging of cutaneous melanocytic lesions. *J Dermatol Surg Oncol* 1989; 15: 854-8.
131. Takahashi M, Kohda H. Diagnostic utility of magnetic resonance imaging in malignant melanoma. *J Am Acad Dermatol* 1992; 27: 51-4.
132. Maurer J, Knollmann FD, Schlums D, *et al.* Role of high-resolution magnetic resonance imaging for differentiating melanin-containing skin tumors. *Invest Radiol* 1995; 30: 638-43.
133. In: Warburg O, ed. *The Metabolism of Tumours*. New York: Richard Smith, 1931.
134. Warburg O, Wind F, Negelein E. On the metabolism of tumours in the body. In: Warburg O, ed. *Metabolism of Tumours*. London: Constable, 1930: 254-65.
135. Som P, Atkins HL, Bandoypadhyay D, *et al.* A fluorinated glucose analog, 2-fluoro-2-deoxy-D-glucose (F-18): Nontoxic tracer for rapid tumor detection. *J Nucl Med* 1980; 21: 670-5.
136. Friedman KP, Wahl RL. Clinical use of positron emission tomography in the management of cutaneous melanoma. *Semin Nucl Med* 2004; 34: 242-53.
137. Brady MS, Kavolius JP, Quan SH. Anorectal melanoma. A 64-year experience at memorial sloan-kettering cancer center. *Dis Colon Rectum* 1995; 38: 146-51.
138. Schuchter LM, Green R, Fraker D. Primary and metastatic diseases in malignant melanoma of the gastrointestinal tract. *Curr Opin Oncol* 2000; 12: 181-5.
139. Kotoulas C, Skagias L, Konstantinou G, *et al.* Primary pulmonary melanoma diagnosis: The role of immunohistochemistry and immunocytochemistry. *J BUON* 2007; 12: 543-5.
140. Bajer-Czajkowska A, Nowacki P. Primary diffuse meningeal melanomatosis. case report. *Neurol Neurochir Pol* 2007; 41: 82-8.
141. Steiber Z, Ehlers N, Heegaard S, Hjortdal J, Berta A, Prause JU. Brown cornea. *Graefes Arch Clin Exp Ophthalmol* 2008; 246 (4): 537-41.
142. Gupta D, Deavers MT, Silva EG, Malpica A. Malignant melanoma involving the ovary: A clinicopathologic and immunohistochemical study of 23 cases. *Am J Surg Pathol* 2004; 28: 771-80.
143. D'Silva NJ, Kurago Z, Polverini PJ, Hanks CT, Paulino AF. Malignant melanoma of the oral mucosa in a 17-year-old adolescent girl. *Arch Pathol Lab Med* 2002; 126: 1110-3.

144. Vlodavsky E, Ben-Izhak O, Best LA, Kerner H. Primary malignant melanoma of the anterior mediastinum in a child. *Am J Surg Pathol* 2000; 24: 747-9.
145. Rohwedder A, Philips B, Malfetano J, Kredentser D, Carlson JA. Vulvar malignant melanoma associated with human papillomavirus DNA: Report of two cases and review of literature. *Am J Dermatopathol* 2002; 24: 230-40.
146. Thompson LD, Wieneke JA, Miettinen M. Sinonasal tract and nasopharyngeal melanomas: A clinicopathologic study of 115 cases with a proposed staging system. *Am J Surg Pathol* 2003; 27: 594-611.
147. Oliva E, Quinn TR, Amin MB, *et al.* Primary malignant melanoma of the urethra: A clinicopathologic analysis of 15 cases. *Am J Surg Pathol* 2000; 24: 785-96.
148. Gupta D, Malpica A, Deavers MT, Silva EG. Vaginal melanoma: A clinicopathologic and immunohistochemical study of 26 cases. *Am J Surg Pathol* 2002; 26: 1450-7.
149. Phelps ME, Schelbert HR, Mazziotta JC. Positron computed tomography for studies of myocardial and cerebral function. *Ann Intern Med* 1983; 98: 339-59.
150. Leskinen-Kallio S, Ruotsalainen U, Nagren K, Teras M, Joensuu H. Uptake of carbon-11-methionine and fluorodeoxyglucose in non-hodgkin's lymphoma: A PET study. *J Nucl Med* 1991; 32: 1211-8.
151. Bailet JW, Abemayor E, Jabour BA, Hawkins RA, Ho C, Ward PH. Positron emission tomography: A new, precise imaging modality for detection of primary head and neck tumors and assessment of cervical adenopathy. *Laryngoscope* 1992; 102: 281-8.
152. Strauss LG, Clorius JH, Schlag P, *et al.* Recurrence of colorectal tumors: PET evaluation. *Radiology* 1989; 170: 329-32.
153. Nagata Y, Yamamoto K, Hiraoka M, *et al.* Monitoring liver tumor therapy with [18F]FDG positron emission tomography. *J Comput Assist Tomogr* 1990; 14: 370-4.
154. Griffeth LK, Dehdashti F, McGuire AH, *et al.* PET evaluation of soft-tissue masses with fluorine-18 fluoro-2-deoxy-D-glucose. *Radiology* 1992; 182: 185-94.
155. Kubota K, Matsuzawa T, Ito M, *et al.* Lung tumor imaging by positron emission tomography using C-11 L-methionine. *J Nucl Med* 1985; 26: 37-42.
156. Hoh CK, Schiepers C, Seltzer MA, *et al.* PET in oncology: Will it replace the other modalities? *Semin Nucl Med* 1997; 27: 94-106.
157. Boni R. Whole-body positron emission tomography: An accurate staging modality for metastatic melanoma. *Arch Dermatol* 1996; 132: 833-4.
158. Gerger A, Koller S, Kern T, *et al.* Diagnostic applicability of in vivo confocal laser scanning microscopy in melanocytic skin tumors. *J Invest Dermatol* 2005; 124: 493-8.
159. Gerger A, Koller S, Weger W, *et al.* Sensitivity and specificity of confocal laser-scanning microscopy for in vivo diagnosis of malignant skin tumors. *Cancer* 2006; 107: 193-200.
160. Gritters LS, Francis IR, Zasadny KR, Wahl RL. Initial assessment of positron emission tomography using 2-fluorine-18-fluoro-2-deoxy-D-glucose in the imaging of malignant melanoma. *J Nucl Med* 1993; 34: 1420-7.
161. Steinert HC, Huch Boni RA, Buck A, *et al.* Malignant melanoma: Staging with whole-body positron emission tomography and 2-[F-18]-fluoro-2-deoxy-D-glucose. *Radiology* 1995; 195: 705-9.
162. Boni R, Boni RA, Steinert H, *et al.* Staging of metastatic melanoma by whole-body positron emission tomography using 2-fluorine-18-fluoro-2-deoxy-D-glucose. *Br J Dermatol* 1995; 132: 556-62.
163. Blessing C, Feine U, Geiger L, Carl M, Rassner G, Fierlbeck G. Positron emission tomography and ultrasonography. A comparative retrospective study assessing the diagnostic validity in lymph node metastases of malignant melanoma. *Arch Dermatol* 1995; 131: 1394-8.
164. Wagner JD, Schauwecker D, Hutchins G, Coleman 3rd JJ. Initial assessment of positron emission tomography for detection of nonpalpable regional lymphatic metastases in melanoma. *J Surg Oncol* 1997; 64: 181-9.
165. Macfarlane DJ, Sondak V, Johnson T, Wahl RL. Prospective evaluation of 2-[18F]-2-deoxy-D-glucose positron emission tomography in staging of regional lymph nodes in patients with cutaneous malignant melanoma. *J Clin Oncol* 1998; 16: 1770-6.
166. Rinne D, Baum RP, Hor G, Kaufmann R. Primary staging and follow-up of high risk melanoma patients with whole-body 18F-fluorodeoxyglucose positron emission tomography: Results of a prospective study of 100 patients. *Cancer* 1998; 82: 1664-71.
167. Holder Jr. WD, White Jr. RL, Zuger JH, Easton Jr. EJ, Greene FL. Effectiveness of positron emission tomography for the detection of melanoma metastases. *Ann Surg* 1998; 227: 764-9; (discussion: 769-71).
168. Eigtved A, Andersson AP, Dahlstrom K, *et al.* Use of fluorine-18 fluorodeoxyglucose positron emission tomography in the detection of silent metastases from malignant melanoma. *Eur J Nucl Med* 2000; 27: 70-5.
169. Acland KM, O'Doherty MJ, Russell-Jones R. The value of positron emission tomography scanning in the detection of subclinical metastatic melanoma. *J Am Acad Dermatol* 2000; 42: 606-11.
170. Swetter SM, Carroll LA, Johnson DL, Segall GM. Positron emission tomography is superior to computed tomography for metastatic detection in melanoma patients. *Ann Surg Oncol* 2002; 9: 646-53.
171. Gulec SA, Faries MB, Lee CC, *et al.* The role of fluorine-18 deoxyglucose positron emission tomography in the management of patients with metastatic melanoma: Impact on surgical decision making. *Clin Nucl Med* 2003; 28: 961-5.
172. Mottaghy FM, Sunderkotter C, Schubert R, *et al.* Direct comparison of [(18)F]FDG PET/CT with PET alone and with side-by-side PET and CT in patients with malignant melanoma. *Eur J Nucl Med Mol Imaging* 2007; 34 (9): 1355-64.